Exhaustion-like dysfunction of T and NKT cells in an X-linked severe combined immunodeficiency patient with maternal engraftment by single-cell analysis

WEI DONG[1*], WENYAN LI[2*], SHAOJIN ZHANG[1], XIAN ZENG[1], QI QIN[1], HUIFENG FAN[2], ZHONGHUI TANG[1], XIA WU[1] and GEN LU[2]

[1]Zhongshan School of Medicine, Sun Yat-sen University, Guangzhou, Guangdong 510080; [2]Department of Respiratory, Guangzhou Women and Children's Medical Center, Guangzhou Medical University, Guangdong Provincial Clinical Research Center for Child Health, Guangzhou, Guangdong 510623, P.R. China

Received September 20, 2022; Accepted January 9, 2023

DOI: 10.3892/ijmm.2023.5228

Abstract. Maternal engraftment is frequently present in X-linked severe combined immunodeficiency (X-SCID) patients caused by pathogenic mutations in *IL2GR*. However, the functional status of the engrafted cells remains unclear because of the difficulty in separately evaluating the function of the maternal and autologous cells. The present study reported an X-SCID patient with a *de novo* c.677C>T (p.R226H) variant in exon 5 of *IL2RG*, exhibiting recurrent and persistent infections from 3-months-old. After the male patient suffering recurrent pneumonia and acute hematogenous disseminated tuberculosis when 13-months-old, single-cell RNA sequencing was applied to characterize the transcriptome landscape of his bone marrow mononuclear cells (BMMNCs). A novel bioinformatic analysis strategy was designed to discriminate maternal and autologous cells at single-cell resolution. The maternal engrafted cells consisted primarily of T, NKT and NK cells and the patient presented with the coexistence of autologous cells of these cell types. When compared respectively with normal counterparts, both maternal and autologous T and NKT cells increased the transcription of some important cytokines (*GZMB*, *PRF1* and *NKG7*) against infections, but decreased the expression of a number of key transcription factors (*FOS*, *JUN*, *TCF7* and *LEF1*) related to lymphocyte activation, proliferation and differentiation. Notably, the expression of multiple inhibitory factors (*LAG3*, *CTLA4* and *HAVCR2*) were substantially enhanced in the T and NKT cells of both origins. In conclusion, both maternal and autologous T and NKT cells exhibited exhaustion-like dysfunction in this X-SCID patient suffering recurrent and persistent infections.

Correspondence to: Dr Gen Lu, Department of Respiratory, Guangzhou Women and Children's Medical Center, Guangzhou Medical University, Guangdong Provincial Clinical Research Center for Child Health, 318 Renmin Road, Guangzhou, Guangdong 510623, P.R. China
E-mail: lugen5663330@sina.com

Dr Xia Wu, Zhongshan School of Medicine, Sun Yat-sen University, 74 Zhongshan Second Road, Guangzhou, Guangdong 510080, P.R. China
E-mail: wuxia23@mail.sysu.edu.cn

*Contributed equally

Key words: X-linked severe combined immunodeficiency, IL2RG mutation, maternal-engrafted cells, single-cell RNA sequencing

Introduction

Severe combined immunodeficiency (SCID) is a rare genetic disease with severe deficiency in both cellular and humoral immunity, resulting in fatal and recurrent opportunistic infections (1-5). X-linked SCID (X-SCID) accounts for 40-60% of SCID cases (1,2), resulting from mutations in the interleukin-2 receptor subunit γ (*IL2RG*) gene on the X chromosome (3,6). IL2RG is a common receptor of interleukins (IL) 2, IL4, IL7, IL9, IL15 and IL21, playing an essential role in lymphocyte development and function (7,8). Mutations in *IL2RG* cause the absence of the protein or altered protein structures, resulting in impaired interactions between the receptor complexes and cytokine ligands, ultimately leading to severe immune deficiency (9). Without the reconstitution of the immune system by hematopoietic stem cell transplantation or gene therapy, X-SCID patients usually die within the first year of life due to recurrent infections (10,11).

Typical X-SCID is characterized by the absence of T cells, a low number of NK cells and a normal to high number of dysfunctional B cells ($T^-B^+NK^-$ phenotype) (5). It was found that ~40% of SCID have maternal engraftment of T lymphocytes due to the patient's unsuccessful recognition and rejection of the maternal blood cells (12). It is hypothesized that maternal T lymphocytes may promote near-term survival in several SCID cases, but SCID patients with and without the maternal engraftment succumb without appropriate reconstitution of the immune system (13,14).

The immunophenotype of engrafted maternal T cells can be diverse, with most cases exhibiting a mature ($CD45RO^+$)

phenotype (15). Functional regulatory T cells are detected within maternal engrafted cells (16) and a massive maternal T cell expansion in response to EBV has been reported (17). However, the engrafted T cells are generally functionally defective, with a restricted T-cell receptor repertoire and limited or no proliferative response to mitogens (12,14,18). Some SCID patients with engrafted maternal T cells are asymptomatic, while others present graft-versus-host disease (GVHD) (14,18,19). Maternal engraftment of B and NK cells are also observed in several cases (17,20-22). Maternal engrafted B cells can cause the monoclonal IgA or IgG1 gammopathy in SCID (20,22), while the function of the maternal NK cells have not been explored in depth (17,22). To the best of the authors' knowledge, there have been no reported cases about maternal engraftment of NKT cells. Overall, the functional status of engrafted maternal cells remains largely undefined due to the difficulty of efficiently separating and characterizing maternal cells and autologous counterparts with the limited number of cells.

The present study applied single-cell RNA sequencing (scRNA-seq) to study the transcriptome landscape of BMMNCs from an X-SCID patient with engrafted maternal cells. A novel analytic strategy was designed to discriminate between maternal and autologous cells. The present study characterized the functional status of autologous and maternal engrafted T and NK-like cells in this X-SCID patient with single-cell resolution. It was hypothesized that the scRNA-seq data from BMMNCs in this X-SCID patient would provide valuable resources for investigating the essential characteristics of heterogeneous immune cells and potentially guide the development of advanced therapies.

Materials and methods

Collection of clinical samples. Peripheral blood (PB), bone marrow (BM), hair follicles and mouth swabs from the X-SCID patient (13-months-old) and PB from the patient's parents were obtained with written informed consent from the patient's parents according to procedures approved by the Guangzhou Women and Children's Medical Center (approval number: 105A01). The PB and BM were processed within two hours of sample collection. Then ~30 hair follicles were collected in a clean 1.5 ml Eppendorf tube and four mouth swabs collected separately in sealed tubes were frozen at -80˚C prior to DNA extraction.

Captured exome sequencing. DNA was extracted from the patient's PB using the QIAamp DNA Blood Mini kit (Qiagen GmbH), following DNA fragmentation, end-repair, A-tailing and ligation to adapters to generate sequencing libraries. Exome-derived DNA fragments within the library were heat denatured and hybridized with biotin probes targeting immune genes (P039-Exome; MyGenostics) and the libraries hybridized with probes were enriched via biotin binding to streptavidin beads (Thermo Fisher Scientific, Inc.) for 45 min at room temperature (RT). After rinsing, the beads were incubated in 0.1 mol/l HCl at RT to denature the DNA, allowing the hybridized DNA fragments eluting from the beads. The enriched DNA fragments were neutralized with equal volume of 0.1 mol/l CH_3COOH, purified with P-30 column (Bio-Rad Laboratories, Inc.), and amplified for exome sequencing.

Sanger sequencing. To verify the mutation at the *IL2RG* locus, Sanger sequencing was performed using the DNA extracted from the PB of the patient and his parents across the mutation site (primers: GTGAGACCCTGCCTCAAAAG and CAG CACATATTTGCCACACC).

Whole-genome sequencing (WGS). The patient's hair follicles and mouth swabs were digested with 0.1 mg/ml proteinase K (Thermo Fisher Scientific, Inc.) in 100 μl 150 mM NaCl with 10 mM EDTA and 1% SDS overnight at 55˚C. The solution was then extracted twice with equal volume of phenol-chloroform-isoamyl alcohol (Thermo Fisher Scientific, Inc.), once with equal volume of chloroform. The solution was then added with 20 μl 7.5 mol/l ammonium acetate and 300 μl absolute ethanol to precipitated DNA. DNA from the PB of the patient's parents was prepared using the QIAamp DNA Blood Mini kit (Qiagen GmbH). The libraries were generated using NEBNext Ultra DNA Library Prep kit for Illumina (New England BioLabs, Inc.).

Chromosomal microarray. DNA extracted from the patient PB was subjected to chromosomal microarray (CMA) analysis using an Affymetrix Cytoscan 750K Microarray kit (Thermo Fisher Scientific, Inc.) according to the manufacturer's instructions. This assay covers 550,000 markers to detect copy number variations and 200,000 high-performing SNP probes. The data of the Cytoscan 750K Microarray were analyzed using Chromosome Analysis Suite version 2.0 (Affymetrix; Thermo Fisher Scientific, Inc.).

Next-generation sequencing and data processing. Exome sequencing libraries and WGS libraries were sequenced using the NextSeq 500 system (Illumina, Inc.) in paired-end 150 bp mode. The raw sequenced reads were filtered for low quality reads and adapter regions using Trimmomatic v.0.39 (23) with the adapter sequences (Read 1: AGATCGGAAGAGCAC ACGTCTGAACTCCAGTCA; Read 2: AGATCGGAAGAG CGTCGTGTAGGGAAAGAGTGT). Cleaned high quality sequencing reads (Q30) were then aligned to the human reference genome (GRCh38) using the Burrows Wheeler Aligner (24) (BWA, version 0.7.15) with default parameters and then sorted using the SAMtools (25) (version 1.10) software. The 'MarkDuplicates' function embedded in Picard (version 1.107, http://broadinstitute.github.io/picard/) was applied to mark and discard PCR duplicates. The results were visualized and displayed using the IGV (26-28) genome browser.

Short tandem repeat (STR) marker detection. DNA extracted from the patient's PB and mouth swabs was subjected to genetic screening at 16 STR loci, covering 14 pairs of chromosomes across the genome. DNA from the patient's mother PB was used as a control.

Fluorescence in situ hybridization (FISH). To verify the mixed cell status of the patient PB, FISH experiments were performed using a Vysis CEP X SpectrumOrange/Y SpectrumGreen Labeled Fluorescent DNA probe kit (Abbott Pharmaceutical Co. Ltd.) with the patient PB, according to the manufacturer's instructions. Briefly, nuclei isolated from the PB were fixed,

denatured and hybridized with the DXZ1 probes (targeting to the X chromosome) and DYZ3 probes (targeting to the Y chromosome). After staining with DAPI at RT for 10 min, nuclei were imaged using a fluorescence microscope. Images of 400 interphase nuclei were evaluated and quantified.

Single-cell RNA sequencing. The BM collected from the patient was treated with 6% Hespan to remove red cells. Mononuclear cells were then enriched by Ficoll gradient centrifugation at RT for 30 min at 800 x g. BMMNCs were rinsed twice and resuspended in PBS (Ca^{2+} free, Mg^{2+} free) supplemented with 0.04% BSA. Cells were then filtered with a 40-μm strainer and stored on ice until processing. Viability (>95%), concentration (1,400 cells/μl), debris (almost none) and aggregation (almost none) ratios were determined using an automated cell counter (Nexcelom Bioscience LLC). According to the manufacturer's manual, the single-cell suspension was loaded onto ChIP B (10x Genomics) with GEM beads from Chromium Single Cell 3' Reagent kit V3 (10x Genomics). In total, two libraries were constructed, each with ~16,000 cells loaded to obtain 10,000 cells. cDNA was amplified for 11 cycles and about 40 ng of purified cDNA (SPRIselect beads, 0.6x) was input for each library construction (12 cycles of index PCR, 0.6x and 0.8x SPRIselect beads for size-selection). Concentrations of cDNA and libraries were measured with Qubit (Thermo Fisher Scientific, Inc.) and their size distribution was determined using Qsep (BiOptic Inc.). Each library was sequenced in the 2x150 bp mode (NovaSeq; Illumina, Inc.) for 100 Gb of data.

Collection of public scRNA-seq datasets. To compare the immune cell features between the X-SCID patient and healthy individuals, the scRNA-seq data of BMMNCs from eight healthy donors (four males and four females) from the HCA data portal (https://data.humancellatlas.org/explore/projects/cc95ff89-2e68-4a08-a234-480eca21ce79) and peripheral blood mononuclear cells (PBMCs) from a 29-year-old healthy male donor from the 10x Genomics website (https://support.10xgenomics.com/single-cell-gene-expression/datasets/3.0.0/pbmc_10k_v3) were collected.

Single-cell RNA-seq data processing. Clean sequencing reads of each sample were mapped to the human reference genome (GRCh38) by STAR with Cell Ranger pipelines (version 3.1.0; 10x Genomics) and the feature-barcode matrices were generated using the 'cellranger count' command with default parameters. The pre-filtered gene expression matrices were analyzed using R (v.3.6.0, https://www.r-project.org/) software (29) with the Seurat package (v.3.2.3, https://satijalab.org/seurat/) (30). Briefly, genes expressed in >3 cells of the data and cells with >200 genes detected were extracted for further analyses. Low-quality cells were removed when >10% of unique molecular identifiers (UMIs; >20% for the PBMC data) were derived from the mitochondria. Gene expression matrices were then normalized and scaled by the 'SCTransform' function.

Multiple dataset integration and batch effect correction. To remove the batch effects across different samples and different versions of reagent chemicals, the integration methods adopted by the Seurat package (v.3.2.3) were employed to assemble multiple scRNA-seq datasets into an integrated and unbatched one. Briefly, a total of 3,000 features with high cell-to-cell variation were identified by the 'SelectIntegrationFeatures' function. 'Anchors' between individual datasets were computed with the 'FindIntegrationAnchors' function and then import to the 'IntegrateData' function to create a batch-corrected expression matrix of all cells.

Dimensional reduction and unsupervised clustering analysis. To reduce the dimensionality of the integrated datasets, the 'RunPCA' function in Seurat was applied with default parameters on linear-transformation scaled data generated by the 'SCTransform' function. Next, the 'ElbowPlot' function was applied to identify the true dimensionality of the dataset. Finally, cells were clustered using the 'FindNeighbors' and 'FindClusters' functions with a resolution of 0.6 and 30 clusters were obtained. Nonlinear dimensional reduction was conducted by the 'RunUMAP' function with dims parameter set to 50 for visualizing the clustering result in 2D space.

Cluster marker analysis and cell type annotation. To annotate the cell type of each cluster, the SingleR package (31) was used to compare the transcriptome of every single cell to the reference immune datasets (NovershternHematopoieticData) (32) to determine cellular identity. To verify the annotation, the expression patterns of the canonical immune cell markers were plotted for manual inspection. The 'FindAllMarkers' function in Seurat was also used to find the top markers for each identified cluster. Finally, 28 out of the 30 distinct cell clusters were assigned to well-known immune cell types and two were assigned as unknown (Unk 1 and Unk 2) due to the lack of distinct features of known cell types.

Discrimination of the maternal and autologous cells. As the *XIST* gene was transcribed exclusively in cells derived from females, the present study first defined that the cells expressing *XIST* (XIST>0, XIST_ON) were from maternal engraftment, whereas those with null *XIST* expression (XIST=0, XIST_OFF) were autologous. Meanwhile, due to the patient containing exclusive *de novo* IL2RG c.677C>T mutation, maternal and autologous cells should be detected on the variant locus as C (consistent with the reference genome, IL2RG_C) and T (variant, IL2RG_T), respectively. Last, based on the expression level of *XIST* and the sequence in the mutation site, the maternal (XIST_ON with IL2RG_C) and autologous (XIST_OFF with IL2RG_T) cells were distinguished.

Classification of the NK and NKT cells. As CD3 genes (except for the *CD247* gene) were expressed only in NKT but not NK cells, the NK-like cells were defined with at least one of the CD3 genes (*CD3E*, *CD3D* and *CD3G*) as NKT and the rest as NK cells.

Differentially expressed genes and functional enrichment. Due to various versions of reagent chemicals, the comparison of BMMNC scRNA-seq data between the X-SCID patient and the normal BMMNCs resulted in highly biased differentiated expression pattern, although integrated analyses of these data sets achieved satisfactory results in cell clustering. Therefore, to conduct unbiased differential expression analysis, the

scRNA-seq data of the X-SCID patient BMMNCs were compared with a scRNA-seq data set using the same reagent chemical version with PBMCs from a healthy donor. The 'FindMarkers' function in Seurat R package was applied with parameter 'test.use='wilcox', logfc.threshold=0.25, min.pct=0.1' and the Benjamini-Hochberg method was used to estimate the false discovery rate (FDR). Differentially expressed genes (DEGs) were filtered using a minimum average log2 (fold change) of 0.25 and a maximum FDR value of 0.05 for the comparison between the patient's and the healthy donor's cells and with a maximum P-value of 0.05 for the comparison between autologous and maternal cells. Gene Ontology (GO) and Kyoto Encyclopedia of Genes and Genomes (KEGG) enrichment of the DEGs was conducted using the 'enrichGO' and 'enrichKEGG' function of the clusterProfiler (v.3.14.3) R package (33). Gene sets were derived from the GO Biological Process Ontology (34,35). The Hiplot website (https://hiplot-academic.com/), a comprehensive web platform for scientific data visualization, was used to visualize the enrichment results (36).

Calculation of exhaustion module scores. The present study calculated the exhaustion scores in cell cluster with six well-defined exhaustion-related markers (*PDCD1*, *HAVCR2*, *LAG3*, *CTLA4*, *TIGIT*, *TOX*) (37-42) to evaluate the potential exhaustion states. The 'AddModuleScore' function in Seurat at single cell level was used to implement the method with default setting.

Single-cell gene set enrichment. To score pathway activities in individual cells, single-cell gene set enrichment was conducted using the 'AUCell_buildRankings' and 'AUCell_calcAUC' function with default parameters from the R package AUCell (43). Gene sets were selected from the MSigDB database (44) and the fraction of the top-ranking genes within the gene sets in each cell was represented as the AUC value.

Flow cytometry. PBMCs of the patient (13-months-old) and his mother were stained with viability dye (eFluor780; cat. no. 65-0865-14; Invitrogen; Thermo Fisher Scientific, Inc.) and antibodies against CD3 (PE/Cy7; cat. no. 300420; BioLegend, Inc.), CD56 (APC; cat. no. 17-0566-42; Invitrogen; Thermo Fisher Scientific, Inc.) and CD16 (FITC; cat. no. 11-0168-42; Invitrogen; Thermo Fisher Scientific, Inc.) or antibodies against CD3 (PE/Cy7; cat. no. 300420; BioLegend, Inc.), TIGIT (PE; cat. no. 12-9500-42; Invitrogen; Thermo Fisher Scientific, Inc.) and CD279 (PD-1, FITC; cat. no. 367412) with the eBioscience intracellular fixation and permeabilization buffer set (cat. no. 88-8824-00; Invitrogen; Thermo Fisher Scientific, Inc.) according to the manufacturer's instruction. Briefly, 1 million PBMCs were fixed in 100 μl IC Fixation Buffer for 30 min at RT and rinsed twice with 200 μl 1X permeabilization buffer. The cells were then resuspended in 50 μl 1X permeabilization buffer with the corresponding primary antibodies (1:100) for 30 min at RT protected from light. The stained cells were analyzed with a 5-laser Cytek Aurora flow cytometer (Cytek Biosciences). The data were analyzed with FlowJo X (v.10.0.7 R2; FlowJo LLC). The low proportion of NK cells would not alter the profile of the total $CD3^+$ T cells.

Statistical analysis. The DEGs were identified using the wilcox test by 'FindMarkers' function in Seurat R package (30), and the Benjamini-Hochberg method was used to estimate the FDR. The GO and KEGG functional enrichment of DEGs were conducted using the one-sided version of fisher's exact test by 'enrichGO' and 'enrichKEGG' function in clusterProfiler R package (33). $P<0.05$ was considered to indicate a statistically significant difference.

Results

Clinical characteristics of the patient. A male infant with prolonged fever and recurrent infections since 3-months-old was hospitalized 4 times from 4-months-old to 13-months-old. On the first admission (at 4-months-old), *Pneumocystis jirovecii*, *Aspergillus* and *Mycobacterium tuberculosis* were detected in the patient's bronchial alveolar lavage fluid and *Cytomegalovirus* (CMV) and *Pneumocystis jirovecii* in his PB. T-SPOT (5-6 months) and *Streptococcus pneumoniae* and *Haemophilus influenzae* (7 months) presented later in the patient's PB (Table I). Pulmonary imaging continuously found multiple patchy and cable/patchy high-density shadows (at 4 months, 5-6 months and 13 months-old) and pneumonia (7 months-old) in the patient (Table I). Since routine blood tests continuously detected a high number of white blood cells ($14.9\text{-}42.9\times10^9$ cells/l) and lymphocytes ($11.18\text{-}28.74\times10^9$ cells/l) in the patient (Table I), the infant was considered to have persistent and recurrent infections. Peripheral immunological profiles revealed that the patient exhibited a $T^+B^+NK^+$ immunophenotype, with normal to high number of $CD3^+$ T cells (1,619 or 5,943 cells/μl) and $CD8^+$ T cells (1,371 or 3,619 cells/μl), normal number of $CD19^+$ B cells (307 or 814 cells/μl) and low to normal number of $CD4^+$ T cells (200 or 2,172 cells/μl) and $CD56^+$ NK cells (105 or 215 cells/μl; Table I). The patient had low to normal levels of IgG but he was administered with IgG injections every month from 4-months-old. Moreover, IgA was always undetectable in the patient and the IgM was also almost absent at the age of 7 months (Table I), indicating the loss of function of most B cells. Genetic screening using the patient's PB (at 5-6 months) detected a c.677C>T variant in exon 5 of the *IL2RG* gene (Figs. 1A and S1A). This is a variant documented as X-SCID-related (ClinVar ID: 225196, https://www.ncbi.nlm.nih.gov/clinvar/; SNPdb: rs869320660, https://www.ncbi.nlm.nih.gov/snp/) (45). Therefore, the patient was diagnosed as X-SCID. Phytohemagglutinin (PHA) stimulation failed to induce the patient's PB cells (at 13 months) into mitosis, irrespective of cell recovery (data not shown). The patient lacked signs of GVHD, such as chronic eczematous dermatitis, marked increase of liver enzyme levels and abnormal bone marrow smear. He received broad-spectrum antibiotics, antifungal and anti-tuberculous therapy. However, he had no chance of hematopoietic stem cell transplantation or gene therapy and succumbed eventually at the age of 15 months old.

Genetic screening of IL2RG mutation in the X-SCID patient. The c.677C>T variant in *IL2RG* was detected heterozygous in the PB of the patient (Figs. 1A and S1A). Intriguingly, whole genome sequencing re-detected the variant but hemizygously in the patient's hair follicles and oral pharyngeal

Table I. Clinical immunologic characterizations of the male X-SCID patient.

	Age				Normal value
	4 months	5-6 months	7 months	13 months	
Infections	Pneumonia	Pneumonia, acute hematogenous disseminated tuberculosis	Acute hematogenous disseminated tuberculosis	Pneumonia, diarrhea, chronic hematogenous disseminated tuberculosis	-
Treatment	IVIG, cephalosporins, azithromycin, caspofungin, sulfamethoxazole, Ganciclovir	IVIG, cephaosporins, sulfamethoxazole, voriconazole, Isoniazid, rifampicin, pyrazinamide	IVIG, meropenem, isoniazid, Rifampicin, Pyrazinamide	IVIG, isoniazid, rifampicin, pyrazinamide	-
Blood Routine Examination					
White blood cells ($x10^9$/l)	15	23.6	42.9	14.9	5-12
Lymphocytes ($x10^9$/l)	12.75	17.46	28.74	11.18	1.55-4.8
Monocytes ($x10^9$/l)	1.05	1.18	2.57	0.45	0.55-0.96
Neutrophils ($x10^9$/l)	1.2	4.72	9.87	3.28	2-7.2
Peripheral immunological profiles					
Serum IgG (g/l)	3.75[a]	ND	6.84[a]	0.55	3.60-9.2
Serum IgM (g/l)	0.45	ND	0.06	0.05	0.38-1.26
Serum IgA (g/l)	<0.07	ND	<0.07	<0.07	0.08-0.56
Serum IgE (IU/ml)	7	ND	<5	5	0-15
$CD3^+$ Abs (cells/μl)	1,619	ND	ND	5,943	805-4,459
$CD3^+CD4^+$ Abs (cells/μl)	200	ND	ND	2,172	345-2,350
$CD3^+CD8^+$ Abs (cells/μl)	1,371	ND	ND	3,619	314-2,080
$CD19^+$ Abs (cells/μl)	307	ND	ND	814	240-1,317
$CD16/56^+$ Abs (cells/μl)	105	ND	ND	215	210-1,514
Laboratory test results					
Virus nucleic acid test	Cytomegalovirus	ND	ND	ND	-
Blood culture	-	ND	*Streptococcus pneumoniae*, *Haemophilus influenzae*	-	
Mycobacterium tuberculosis DNA test of blood	Negative	T-SPOT (Positive)	ND	ND	-
Blood culture	Negative	Negative	ND	ND	-
PMseq-High throughput gene test of blood	*Pneumocystis jirovecii*	ND	ND	ND	-
PMseq-High throughput gene test of BALF	*Pneumocystis jirovecii*, *Aspergillus*, *Mycobacterium tuberculosis*	ND	ND	ND	-
CT scan	Patchy and cable strip high density shadow	Multiple patchy and patchy high-density shadows	Pneumonia	Multiple patchy and patchy high-density shadows	-
Captured-exome sequencing of blood	-	*IL2RG* gene c.677C>T (exon 5)	-	-	-
Vaccines	At birth: BCG vaccine, first dose of hepatitis B vaccine				

[a]The patient was administered with IgG injections every month and the two tests were conducted shortly post the IgG injection. Abs, absolute; ND, not done; NK, natural killer cells; IVIG, intravenous immunoglobulin; BALF, bronchial alveolar lavage fluid; BCG, Bacillus Calmette Guerin; -, not available.

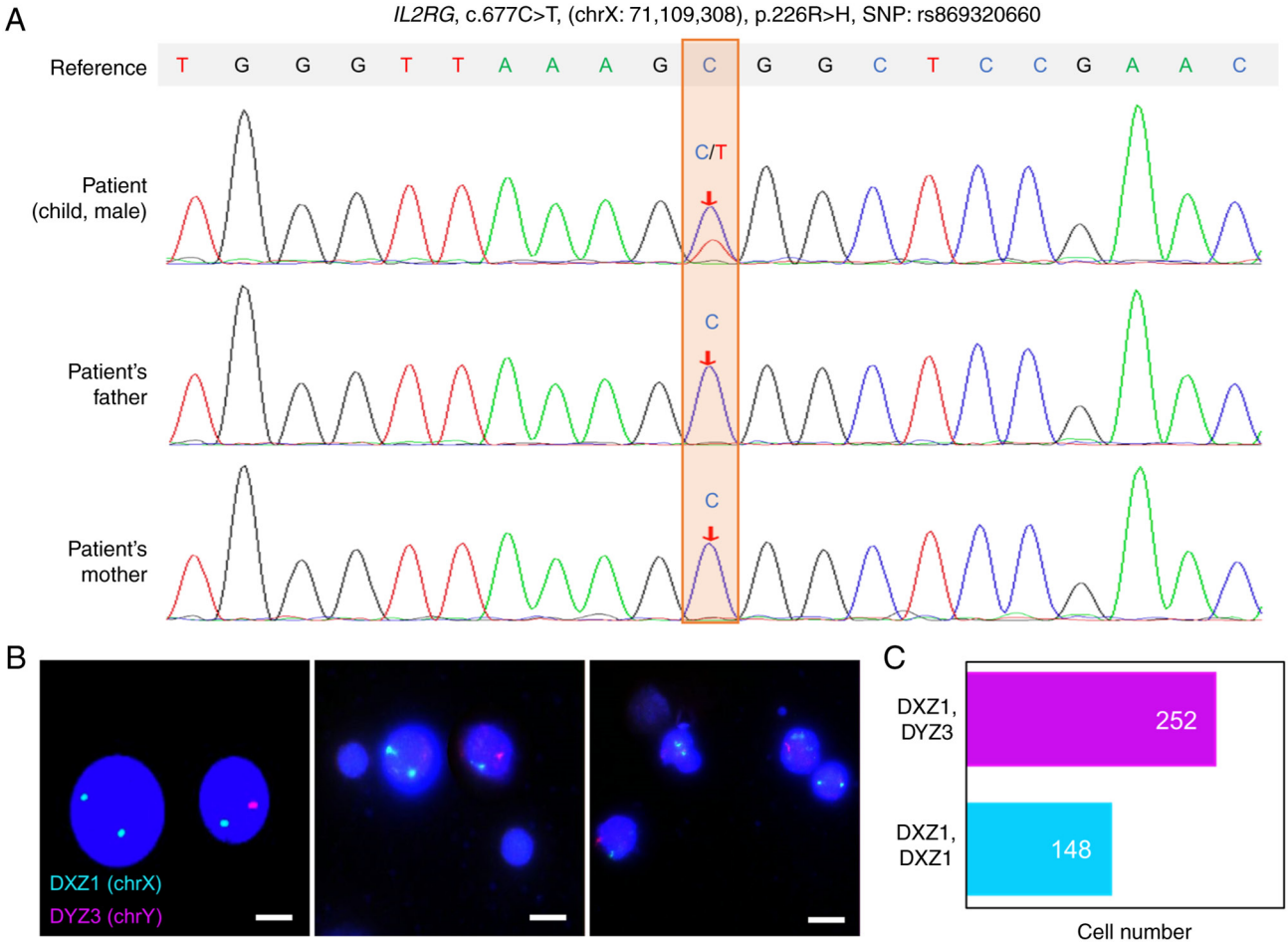

Figure 1. An X-SCID patient with *IL2RG* mutation and maternal cell engraftment. (A) The *de novo* c.677C>T mutation was detected by Sanger sequencing. The heterogeneous C>T mutation in the patient was highlighted in the orange rectangle. (B) The two cells derived from male and female were detected in the peripheral blood of the X-SCID patient. DXZ1 and DYZ3 probes chromosome X and Y, respectively. Scale bar, 10 μm. (C) Quantification of the cells with XY (DXZ1, DYZ3) and XX (DXZ1, DXZ1) karyotype in (B). X-SCID, X-linked severe combined immunodeficiency.

cells (Fig. S1B and C). Therefore, it was suspected the patient harbored maternal engrafted cells, a phenomenon frequently occurred in the X-SCID. This hypothesis was confirmed by chromosome microarray analysis (Fig. S1D) and FISH (Fig. 1B), with ~1/3 of the patient's PBMCs presenting XX genotype (Fig. 1C). STR genetic marker testing also confirmed a maternal origin of the engrafted cells (Table SI). Collectively, a variant in the *IL2RG* gene was found in an X-SCID patient with maternal cell engraftment. A reported case with the same c.677C>T variant in *IL2RG* exhibited low number of T cells phenotype (45), in contrast to the patient in the present study.

Single-cell transcriptional landscapes of BMMNCs in the X-SCID patient. Single-cell RNA sequencing was performed with BMMNCs from the patient (at 13-months-old) to systematically evaluate the states and functions of all types of X-SCID immune cells, including undifferentiated hematopoietic cells. This obtained ~4,000 UMIs and 1,500 genes for each cell (Table SII), indicating sufficient coverage and representative transcripts for subsequent analyses.

The sequencing data were comprehensively analyzed in combination with public available scRNA-seq data of BMMNCs and PBMCs from healthy donors and 230,525 cells passed quality control for unsupervised clustering (Fig. S2A and Tables SII and SIII). Cells from different individuals were well overlapped (Fig. S2B), suggesting the proper elimination of potential batch effects among the different samples. Overall, 30 distinct cell clusters were obtained (Fig. 2A and Table SIV). Each cluster was annotated according to the most variably expressed genes (Fig. S2C and Table SV) and canonical cell-type markers (Fig. 2B and C and Table SVI). The cluster identity was further verified with reference datasets of human immune cells (31) (Fig. S2D). Finally, 28 clusters were assigned with well-defined immune cell identities, including B cells, T cells, NK-like cells, monocytes, dendritic cells, platelet cells, erythrocytes and progenitor and stem cells (Fig. 2A). T and NK-like cell clusters were further manually annotated based on the expression of well-known T and NK cell markers (Fig. S3).

Discrimination of cell sources in the X-SCID patient at the single-cell level. As the maternal cells did not contain *IL2RG* mutation, but autologous cells did, it was hypothesized that cells of the two origins would be at different immune states in this X-SCID patient. The expression profile with single-cell precision provided an unprecedented opportunity to discriminate and characterize separately the maternal engrafted cells and autologous cells in this X-SCID patient. To this end, a novel strategy was designed to discriminate the cell sources

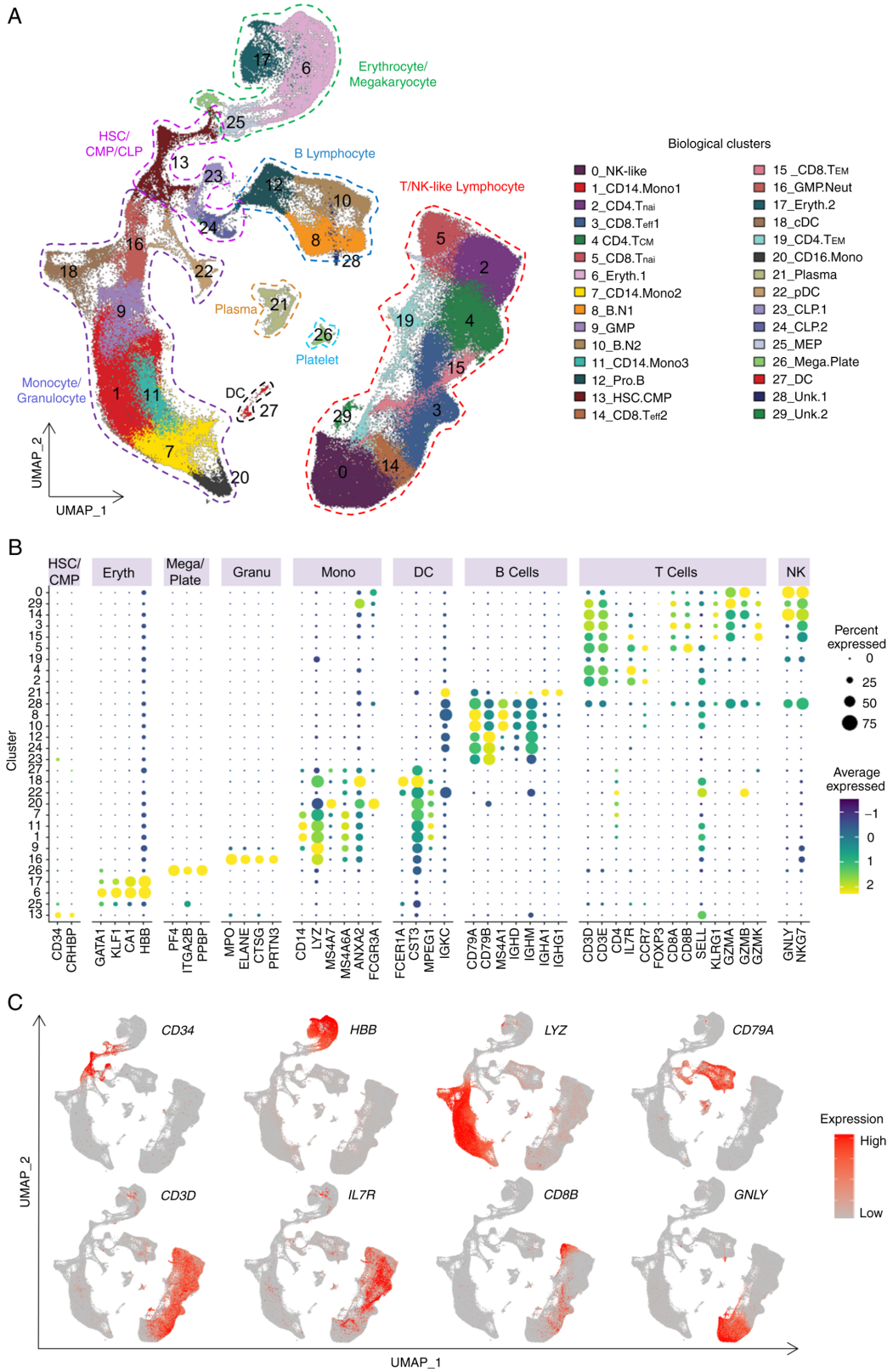

Figure 2. Single-cell transcriptome landscape of the X-SCID patient BMMNCs. (A) BMMNCs from this X-SCID patient and BMMNCs and PBMCs from healthy donors were projected into the UMAP analysis showing 30 cell clusters. Each dot denotes an individual cell and colors represent the cluster origins. The annotation of each cluster is listed on the right. The cell number in each cell cluster from each sample is listed in Table SIV. (B) Dot plot representing the relative average expression of representative marker genes (x-axis) across all clusters (y-axis). As indicated on the legend, the dot size denotes the percentage of cells in a cluster expressing the gene. Dot color represents the relative average expression level. (C) Single-cell transcription levels of representative genes illustrated in the combined UMAP plot. The transcription levels are color-coded: Gray, not expressed; red, expressed. X-SCID, X-linked severe combined immunodeficiency; BMMNCs, bone marrow mononuclear cells; PBMCs, peripheral blood mononuclear cells; UMAP, uniform manifold approximation and projection; HSC, hemopoietic stem cell; CMP, common myeloid progenitor; CLP, common lymphoid progenitor; GMP, granulocyte-macrophage progenitor; MEP, megakaryocyte-erythroid progenitor; Eryth, erythrocytes; Neut, neutrophilic; Mega, megakaryocyte; Plate, platelet; Mono, monocytes; cDC, conventional dendritic cell; pDC, plasmacytoid dendritic cell; NK-like, natural killer like cells; nai, naive; B.N, naïve B cells; eff, effector; CM, central memory; EM, effector memory; Pro, progenitor. Unk, unknown.

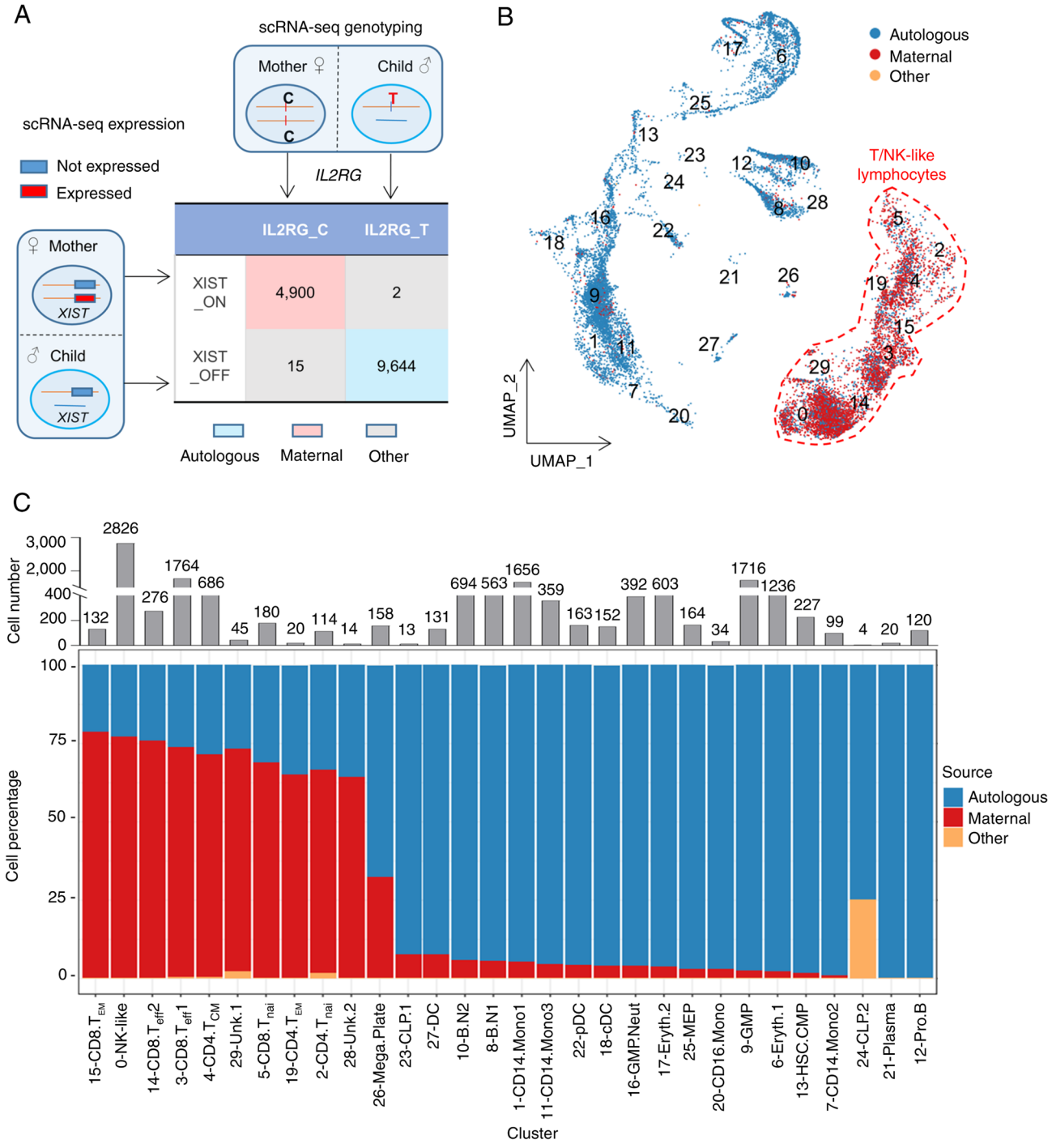

Figure 3. Single-cell level discrimination of cell sources in X-SCID patient BMMNCs. (A) Strategy to discriminate autologous and maternal cells in this X-SCID patient BMMNCs. (B) UMAP plot of BMMNCs in the X-SCID patient with cells color-coded from different cell sources. The T and NK-like lymphocytes were highlighted in the red irregular pattern. (C) The cell number and composition of cell sources in each cluster in the X-SCID patient's BMMNCs. Top, the cell number in each cluster; bottom, the percentage of cells from each cell source in each cluster, colors represent cell sources. X-SCID, X-linked severe combined immunodeficiency; BMMNCs, bone marrow mononuclear cells; UMAP, uniform manifold approximation and projection.

of the patient BMMNCs based on the expression of *XIST* and the existence of the *IL2RG* variant (Figs. 3A and S4A). *XIST* is a highly transcribed gene which mediates X chromosome inactivation (46,47), thus it is expressed exclusively in cells derived from females. The present study defined that the cells expressing *XIST* (XIST_ON) were from maternal engraftment, whereas those with null *XIST* expression (XIST_OFF) were autologous (Fig. S4B and Table SVII). The expression patterns of *XIST* in all samples confirmed the accuracy of this criteria (Fig. S4C). Meanwhile, due to the patient exclusive *de novo IL2RG* c.677C>T mutation (Figs. 1A and S1C), maternal and autologous cells should be detected on the variant locus as C (consistent with the reference genome, IL2RG_C) and T (variant, IL2RG_T), respectively (Fig. S4D). The high consistency between the XIST_ON (XIST_OFF) category and the IL2RG_C (IL2RG_T) subpopulation (Fig. 3A) confirmed that both strategies efficiently and accurately discriminate the cell sources.

To achieve on optimal discrimination of the cell sources, maternal engrafted cells were determined to be simultaneously XIST_ON and IL2RG_C (4,900 cells), while autologous cells were determined to be both XIST_OFF and IL2RG_T (9,644 cells) (Fig. 3A), with the cell origin ratio consistent with that in PBMCs (148 XX:252 XY, Fig. 1C). A total of 17 cells failed in the cell source identification (defined as 'Other'), probably due to an inadequate sequencing depth and/or sequencing errors, which were excluded in the subsequent analyses (Figs. 3, S4E and Table SVIII). The maternal engrafted cells were primarily from the T and NK-like cell groups but merely negligible in the remaining cell clusters (Fig. 3B, C and Table SIX). The effector memory T cells (Cluster 15) harbored the highest ratio (78.79%) of maternal cells (Fig. 3C and Table SIX), which might contribute to the maintenance of the maternal T cells in the patient. Notably, it was found that the common lymphoid progenitor cells (Cluster 23 and 24) were almost exclusively autologous (Fig. 3C), similar with the finding that maternal HSCs were not engrafted into the patient bone marrow (22). Meanwhile, progenitor B cells (Cluster 12) and plasma cells (Cluster 21) were also mainly from autologous sources and thus were not analyzed further.

Cell status across maternal and autologous T and NK-like cells in the X-SCID patient. In general, the T cells detected in X-SCID patients are mostly from maternal engraftment (12,16,22). In the present study, the co-existence of both maternal and autologous T and NK-like cells in this X-SCID patient together with the single-cell level discrimination of cell sources provided a unique opportunity to separately elucidate the functional status of T and NK-like cells from both sources in the same individual. Cell source discrimination revealed that maternal cells were more abundant than autologous ones within the T and NK-like cells (Fig. 4A and B and Table SIX). Differential analyses in clusters with >50 cells in each origin (Cluster 0, 3, 4, 5 and 14) detected the *XIST* gene as the most significantly DEG in all maternal engrafted cells (Fig. S5), confirming the efficiency of the cell origin separation. Multiple genes were differentially expressed in a $CD8^+$ effector T cell population (Cluster 14), including maternally enhanced *IKZF3* and *TGFBR3* and autologously enriched *GZMK*, *TNFAIP3*, *JUN* and *NFATC3* (Fig. 4C and Table SX). GO enrichment analyses of the DEGs revealed that the autologously upregulated genes in Cluster 14 were enriched in multiple immunity-related signaling pathways, especially the NOD-like receptor signaling pathway and Toll-like receptor signaling pathway (Fig. 4D), indicating a function against infections of the patient autologous cells. Notably, cells of both origins showed an enrichment in the PD-L1 expression and PD-1 checkpoint pathway (Fig. 4D). Other clusters showed similar transcriptome between cells of the two sources, except for some DEGs in the $CD8^+$ naïve cells (Fig. S5A). Taken together, the majority of maternal engrafted cells in the patient exhibited a similar cell status to that of autologous counterparts, with differentially expressed genes mainly in a $CD8^+$ effector T cell population.

Characterization of T cells in the X-SCID patient BMMNCs. T and NK-like cells in this X-SCID patient were primarily (65.0-78.79%) of maternal source (Fig. 3C and Table SIX). To further characterized the status and function of the maternal and autologous T cells in the patient, the cells in T cell clusters were compared with >50 cells in each cell origin respectively with the counterpart from the scRNA-seq data of a healthy donor collected in the 10x Genomics dataset (Figs. 5A and S6A). The DEG patterns were similar across cell origins and cell clusters in the patient (Fig. S6A and B and Tables SXI and SXII). Fig. 5B presents the average expression levels of the DEGs common in cells of both origins and in all clusters, except for *SELL* which was maternally highest-expressed in Cluster 14 (Fig. S6B and Table SXIII). A number of genes related to antigen presentation and inflammatory effects (*HLA-DPA1*, *HLA-DPB1*, *GZMB* and *PRF*) were higher expressed in both autologous and maternal cells (Fig. 5B), reflecting the immune reaction of the patient to fight against severe and continuous infections. Accordingly, type I interferon response genes, such as *IFITM1* and *IFI27*, tended to be expressed at higher levels in the patient (Fig. 5C). However, a number of transcription factors (TFs) that are important for T cell proliferation, differentiation and maturation (*FOS, TCF7, LEF1* and *MYC*) (48-51) were significantly attenuated in the patient (Fig. 5B and C), accounting for the fact that T cells were not properly differentiated and matured in the X-SCID patients (52).

To comprehensively understand the nature of the T cell status and function, GO enrichment analyses of the DEGs revealed that the patient-upregulated genes were enriched in biological processes such as T cell activation, response to interferon-γ and antigen processing and presentation, reflecting an active immune response in the patient (Fig. 5D). The patient-downregulated genes were prone to processes of T cell activation and differentiation, regulation of cell-cell adhesion and regulation of lymphocyte activation (Fig. 5E), indicating T cell dysregulation in the activation and differentiation in this X-SCID patient.

Characterization of NK-like cells in the X-SCID patient BMMNCs. The NK-like cells contained two cell types, NK and NKT cells, which were similar in the expression pattern of CD56 (*NCAM1*) and CD16 (*FCGR3A*), but differed in the expression of CD3 (Fig. S7A). Flow cytometry results also showed the existence of the NK (Fig. S7B) and NKT (Figs. 6A and S7C) cells in the PB of the patient and his mother. The NK-like cells in Cluster 0 were then classified into NK [45 (autologous)/110 (maternal), 1.1% of 14,561 (total) and NKT [596 (autologous)/2,072 (maternal), 18.3% of 14,561 (total)]; Figs. 6B, S7D and Table SXIV]. Moreover, the expression of CD16 and CD56 in the maternal cells confirmed the existence of maternal engrafted NKT (Fig. S7E) and NK (Fig. S7F) cells in the patient. As neither NKT (Fig. S7G) nor NK (Fig. S7H) cells presented DEGs other than *XIST* between autologous and maternal cells, cells of the two origins were combined in each cluster to compare with the counterpart cells from the normal donor [520 (NKT)/237 (NK), 4.7% (NKT)/2.2% (NK) of 10,964 (total); Figs. 6B, S7D and Table SXIV]. Nevertheless, the expression level of DEGs in autologous, maternal and healthy NKT were showed separately (Fig. 6C and D and Table SXV) and NK (Fig. S8A and B and Table SXVI) cells.

A number of DEGs were detected in the patient's NKT and NK cells when compared with the normal counterpart. The *CD8A* up-regulation (Fig. 6C) in the patient's NKT may reflect

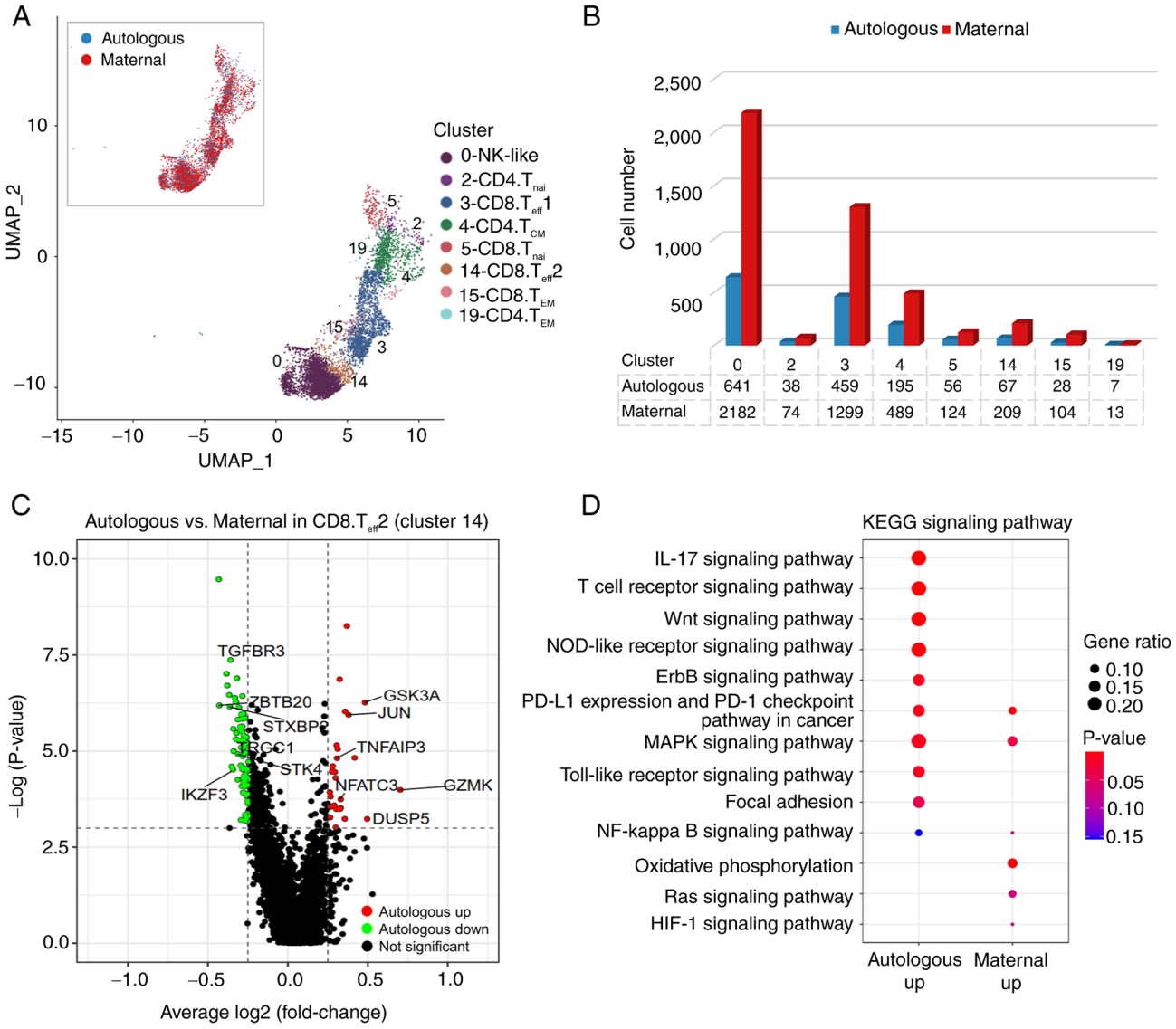

Figure 4. Comparison of the maternal and autologous T and NK-like cells in the X-SCID patient. (A) UMAP plot of the T and NK-like cell clusters in the X-SCID patient's BMMNCs. Each dot denotes an individual cell and colors represent the cluster origin as denoted in Fig. 2A. Top left insert, UMAP plot of the T and NK-like cells in the X-SCID patient's BMMNCs with cells color-coded from different cell sources. (B) The cell number in each cluster of the T and NK-like cells in this X-SCID patient BMMNCs based on cell sources. (C) Volcano plot showing the DEGs between the maternal and autologous cells in Cluster 14 of T cells. The red and green dots represented genes expressed specifically higher in autologous and maternal cells, respectively and the black dots represented genes not differentially expressed. Representative DEGs are labelled. (D) Bubble plot showing the signaling pathways with KEGG enrichment for genes differentially upregulated in maternal and autologous cells, respectively. X-SCID, X-linked severe combined immunodeficiency; UMAP, uniform manifold approximation and projection; BMMNCs, bone marrow mononuclear cells; DEGs, differentially expressed genes; KEGG, Kyoto Encyclopedia of Genes and Genomes.

an increase of $CD8^+$ NKT cells due to infections (53). As in T cells, a number of genes related to antigen presentation and inflammatory effects (*HLA-DPA1*, *HLA-DPB1*, *GZMH* and *CXCR4*) and type I interferon responses (*IFI27*, *IFITM1* and *IFI6*) were more abundant in the patient's NKT (Fig. 6C-E) and NK (Fig. S8A-C) cells. This suggest that both NKT and NK cells exerted a function to defense against persistent infections in the patient. However, the expression levels of some effector molecules (e.g. *KLRG1*, *FCER1G*, *KLRB1* and *LYZ*) decreased dramatically in the patient's NKT (Fig. 6D and E) and NK (Fig. S8B and C) cells, suggesting an insufficient function of these immune cells. The expression of TFs such as *FOS*, *FOSB*, *JUN* and *CEBPD* also decreased obviously in the patient's NKT (Fig. 6D and E) and NK (Fig. S8B and C) cells. Notably, there were only 45 autologous NK cells, thus the findings within this cell type require further confirmation. Taken together, both maternal and autologous NKT, and probably also NK cells, in this X-SCID patient were dysfunctional, which may also be related to the X-SCID clinical symptoms in the patient.

GO enrichment analyses of the DEGs revealed that the genes upregulated in the patient's NKT cells were enriched in biological processes of type I interferon signaling pathway, antigen processing and presentation and virus defense response, consistent with the immune reaction against the infections. Meanwhile, the patient's NKT-downregulated genes were more frequently detected in biological processes such as T cell activation, response to IL-12 and neutrophil

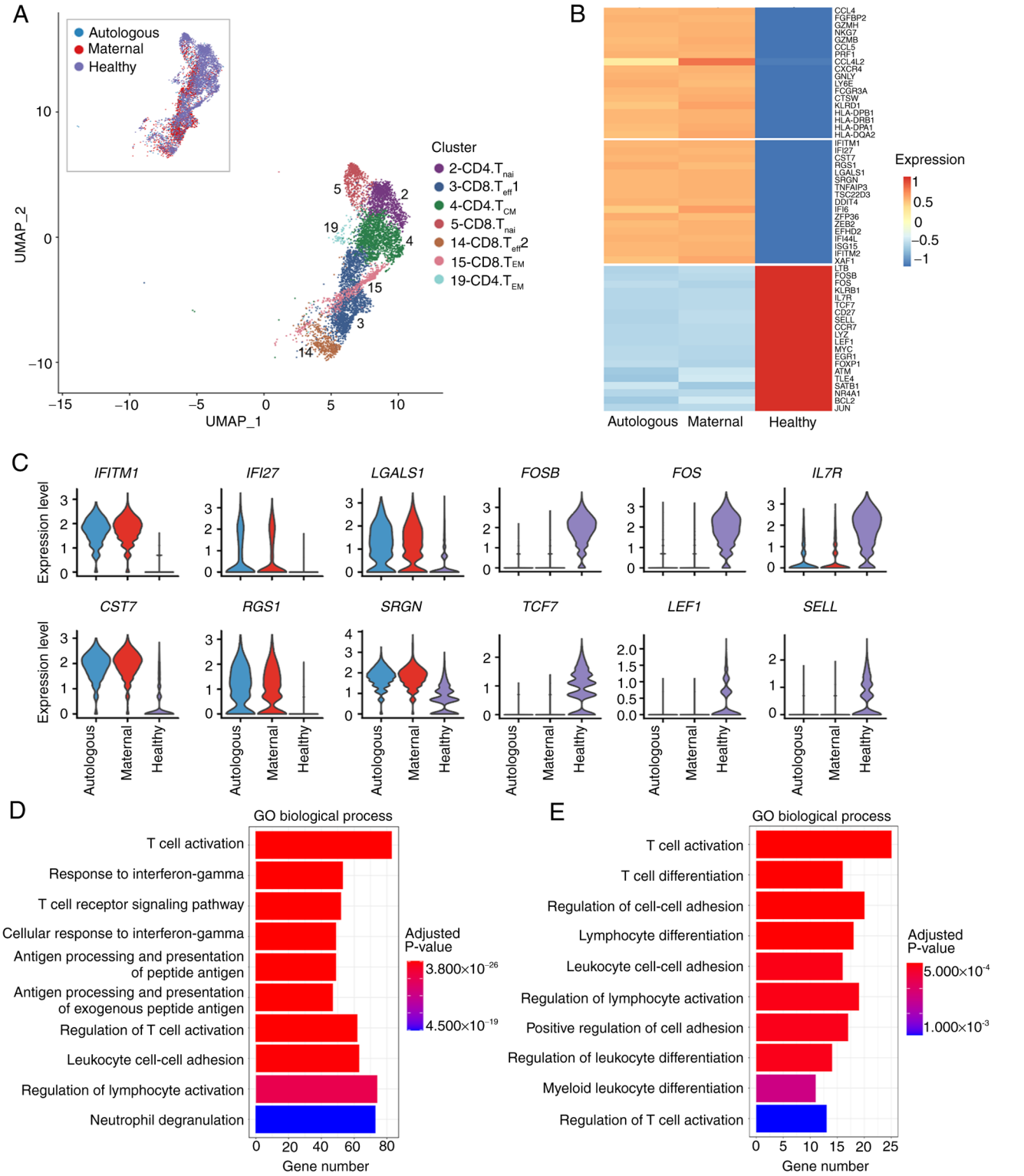

Figure 5. Characterization of T cells in the X-SCID patient's BMMNCs. (A) UMAP plot projecting the T cell clusters from the X-SCID patient and the healthy donor. Each dot denotes an individual cell and colors represent the cluster origin as denoted in Fig. 2A. Top left insert, UMAP plot of the T cells in the X-SCID patient and the healthy donor with cells color-coded from different cell sources. (B) Heatmap displaying the average expression level of common DEGs in maternal and autologous cells when compared respectively with the healthy donor. (C) Violin plot showing representative DEGs in either the X-SCID patient or the healthy donor. Bar plot showing the top 10 GO biological processes enriched in the genes differentially (D) upregulated or (E) downregulated in the X-SCID patient's T cells. X-SCID, X-linked severe combined immunodeficiency; BMMNCs, bone marrow mononuclear cells; UMAP, uniform manifold approximation and projection; DEGs, differentially expressed genes; GO, Gene Ontology.

activation (Fig. S9), reflecting the inability of NKT cells to exert complete immune function. Overall, the data suggested the patient's NKT cells were fighting against the infections, but the dysfunctional cell state confined their capability to efficiently eliminate the infections, which could also facilitate recurrent and continuous infections in the patient.

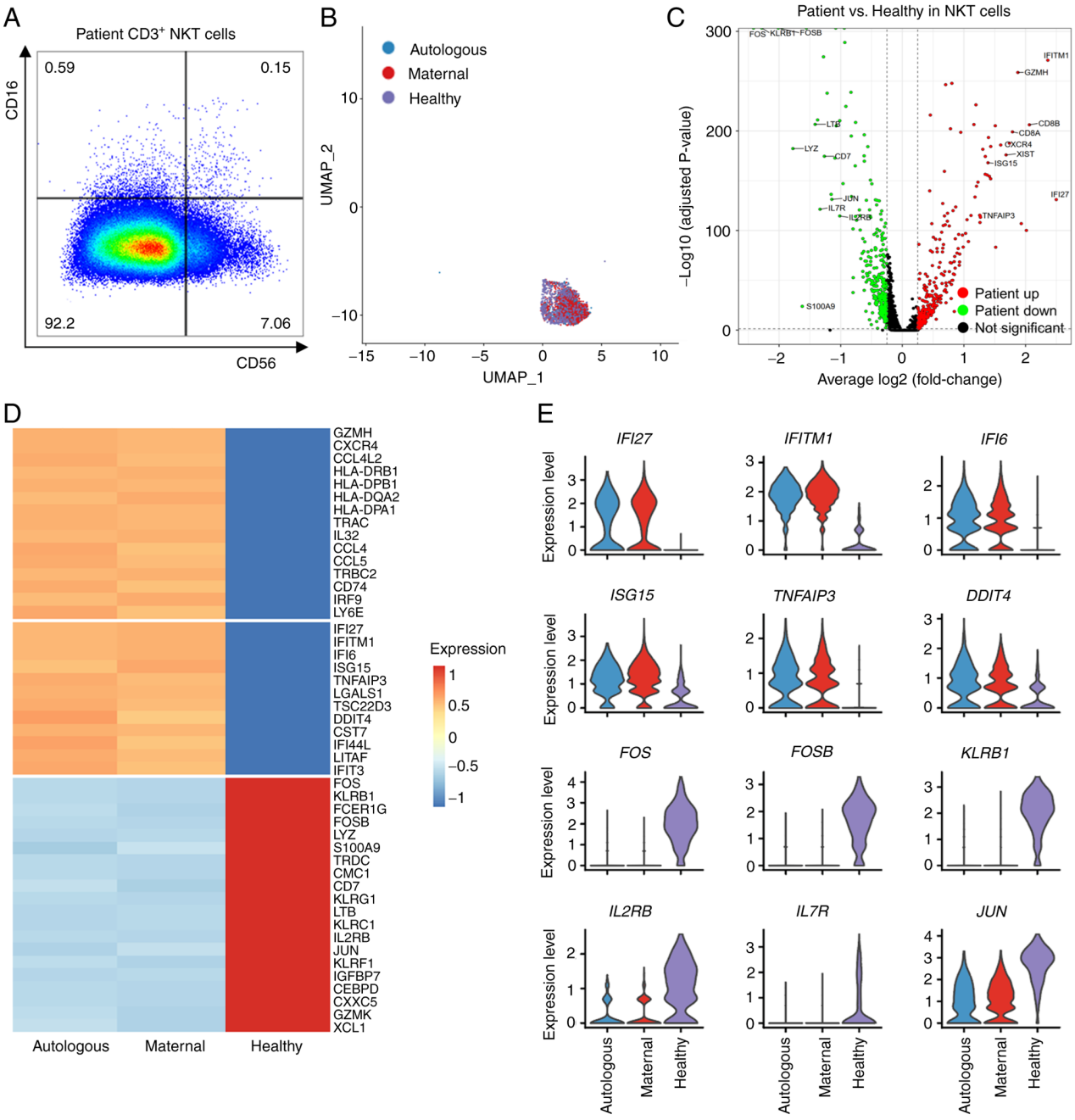

Figure 6. Characterization of NKT cells in the X-SCID patient's BMMNCs. (A) CD16 and CD56 levels of CD3+ NKT cells in the X-SCID patient. The NKT cells were positive with CD16 and/or CD56. (B) UMAP plot projecting the NKT cells from the X-SCID patient and the healthy donor. Each dot denotes an individual cell and colors represent the cell sources. The cell number in each origin was listed in Table SXIV. (C) Volcano plot showing the DEGs between this X-SCID patient and the healthy donor. The red and the green dots represented genes higher expressed in the X-SCID patient and in the healthy donor, respectively and the black dots represented genes not differentially expressed. The representative DEGs were highlighted and labeled. (D) Heatmap displaying the representative DEGs between the X-SCID patient and the healthy donor. (E) Violin plot showing the representative DEGs top expressed in either the X-SCID patient or the healthy donor. X-SCID, X-linked severe combined immunodeficiency; BMMNCs, bone marrow mononuclear cells; UMAP, uniform manifold approximation and projection; DEGs, differentially expressed genes.

Exhausted-like T and NKT lymphocytes in the X-SCID patient. To examine the dysfunctional status of T and NKT cells in this X-SCID patient, some key immune signatures relative to immunity activity were next explored. The analyses confirmed that the patient specifically increased expression of a number of cytotoxic cytokines (*NKG7*, *GZMA*, *GZMB*, *GNLY*, *PRF1* and *IFNG*), with exceptions of *IFNG*, *GZMA* and *GNLY* in the patient's NKT cells (Fig. 7A). However, co-stimulatory factors including *TNFRSF4*, *TNFRSF18*, *CD27*, *CD28* and *CD40LG* were notably decreased in the patient's cells (Fig. 7A). Thus, the patient's T and NKT cells were probably incapable of being sufficiently activated. To this end, the patient's T and NKT cells expressed a lower level of a number of effector molecules like *LYZ* (Figs. 5B and 6D) and were unable to efficiently eliminate the infections.

Next, the present study explored how T and NKT cells became dysfunctional in the patient. Multiple key transcription factors, such as *FOS*, *JUN*, *TCF7* and *LEF1*, are involved

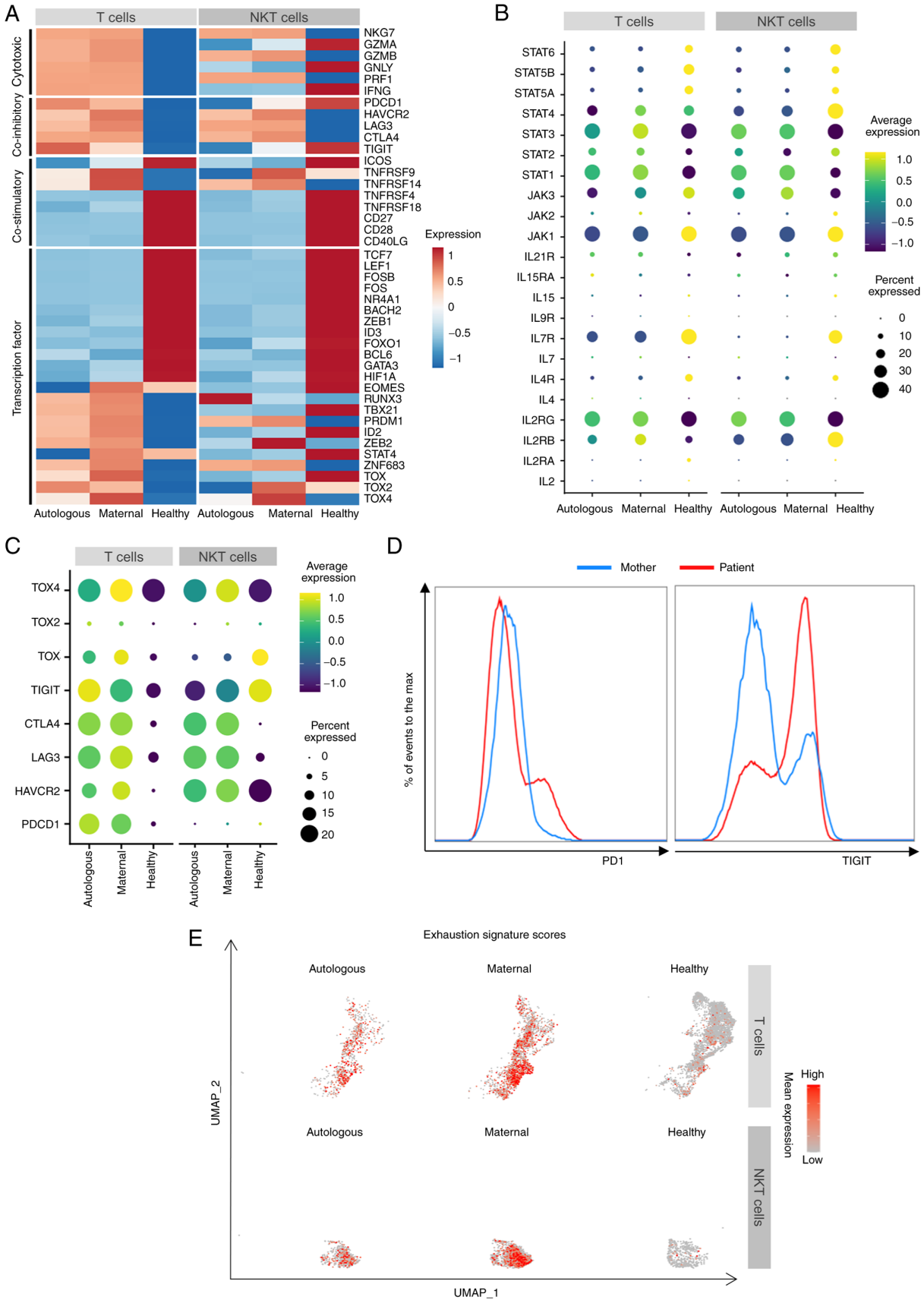

Figure 7. Exhausted-like T and NKT cells in the X-SCID patient. (A) Heatmap showing the average expression levels of representative immune signature genes in T and NKT cells of this X-SCID patient and the healthy donor. (B) Dot plot displaying the average expression levels of *IL2RG* and JAK-STAT related genes in T and NKT cells of the X-SCID patient and the healthy donor. As indicated on the legend, dot size denotes the percentage of cells in a cluster expressing the gene. Dot color represents the relative average expression level. (C) Dot plot displaying the average expression levels of exhaustion-related genes in T and NKT cells of the X-SCID patient and the healthy donor. Dot size and dot color denote the same information as in (B). (D) PD1 and TIGIT levels in T cells of the X-SCID patient and his mother. (E) UMAP plot showing the exhaustion scores in T and NKT cells. X-SCID, X-linked severe combined immunodeficiency; UMAP, uniform manifold approximation and projection.

in lymphocyte proliferation, differentiation and immune responses (48-51), but they were notably downregulated in the patient's T and NKT cells (Fig. 7A), which may contribute to the inability of peripheral blood cells to proliferate upon PHA stimulation. As *BCL2* expression is regulated by *FOS* and *JUN* (54,55), the lower level of *BCL2* in the patient's T cells (Fig. 5B) could be attributed to the attenuated *FOS* and *JUN* expression in these cells. As *FOS* and *JUN* are regulated via the JAK-STAT signaling pathway (48,49), the expression pattern of JAK-STAT-related genes were examined and it was found that *IL7R*, *JAK1*, *STAT5A*, *STAT5B* and *STAT6* were downregulated, while *IL2RG*, *STAT1* and *STAT3* were upregulated in the patient's T and NKT cells from both sources (Fig. 7B). *IL2RB* and *STAT2* were increased in the patient's T but decreased in his NKT cells. By contrast, *JAK3* expression was decreased in the patient's T but increased in NKT cells. *STAT4* levels were lower in the patient's T and NKT cells, except for the higher levels in maternal T cells (Fig. 7B). Moreover, IL2RG ligands, especially IL2 secreted by activated T cells, were expressed at a negligible level (Fig. 7B). These abnormalities indicated a dysregulation of the JAK-STAT pathway, which impaired the expression of key transcription factors mediating lymphocyte proliferation, differentiation and immune responses, leading to the dysfunction of T and NKT cells of both origins in the patient.

Further analyses revealed that the patient's T and NKT cells of both origins enhanced the expression of multiple exhaustion-related inhibitory genes, such as *HAVCR2* and *CTLA4,* and especially *LAG3* (37-39,56) and the transcriptional factor *TOX4* (Fig. 7A and C). Moreover, *TIGIT* and *PDCD1* expression levels were higher in the patient's T cells (Fig. 7A and C), as confirmed with by flow cytometry of the patient's peripheral blood (Fig. 7D). Notably, the expression levels of some inhibitory molecules varied in the maternal and autologous T and NKT cells in the patient. For example, *PDCD1* was slightly more transcribed in autologous T cells. *TIGIT* was higher in autologous T cells, but lower in autologous NKT cells. In addition, the enrichment score of canonical exhaustion markers were higher in the maternal T and NKT cells (Fig. 7E). Taken together, the T and NKT cells were at an exhausted-like dysfunction status post a long-term recurrent pathogen infection in this X-SCID patient.

Discussion

The variant c.677C>T (p.R226H) on the *IL2RG* gene was documented in the ClinVar database (Variation ID: 225196) as a pathogenic variation causing X-SCID. Several studies have reported patients with this particular variant presenting with low number of T cells and B^+NK^- or B^+NK^+ phenotype, but did not describe the maternal engraftment in detail (57-63), although it is a general phenomenon in SCID patients (12). The functional status of the engrafted cells remains largely unclear since the traditional cell separation methods, such as flow cytometry and magnetic bead separation, were not able to separate the cell origins effectively. Moreover, since the maternal engrafted cells may consist of more than one cell type and/or cell state (12,16,17,22), separation and analysis of cells merely based on cell sources (depending on HLA) (12) would confine the systematics evaluation of the cell status of multiple cell types.

The present study applied the state-of-art single-cell technology to study systematically the transcriptome landscape of BMMNCs from a 13-months-old male X-SCID patient with maternal engraftment caused by a *de novo* c.677C>T mutation in the *IL2RG* gene. This allowed the present study to discriminate the maternal engrafted and autologous cell origins and characterize their functions/states with single-cell resolution. It first tried to use published approaches like 'Souporcell' (64) to determine the cell origin based on SNPs, but shortly realized the SNPs between the autologous and maternal cells were heterozygous and represented a low density in genome with sparse read coverage, which confined the efficiency of cell separation. The present study thus designed a novel analytical strategy to effectively distinguish the cell origins of BMMNCs in this X-SCID patient based on the exclusive maternal expression of the *XIST* gene and the autologously specific *de novo* mutation on *IL2RG* and successfully achieved high confidence in cell source discrimination.

The present study detected both autologous and maternal engrafted T, NKT and NK cells in this X-SCID patient. Usually, engraftment of the maternal T cells is the most frequent and was detected in 62% of the B^- SCID and in 50% of the B^+ SCID (12). These T cells were generally defective in immunity function and limited or no proliferative response to mitogens (12,14,18), in consistent with the absent cell proliferation of the patient's T cells upon PHA. The exclusively autologous HSCs and CLP cells in the patient probably gave rise to the patient's autologous T cells. The higher expression of *EOMES* in maternal T cells (Fig. 7A) and the highest maternal cell ratio in the effector memory T cell cluster indicated that the maternal T cells were maintained in the patient probably due to the engraftment of memory T cells, but not naive T cells, as described in the previous studies (14,65).

Previous studies typically characterized SCID based on the effects of classical T, B and NK cells (1,3,15-17,20-22), but did not focus on NKT cells. The present study found NKT dysfunction in cytotoxicity and immune regulation in this X-SCID patient. Further study with more cases is required to verify if the NKT dysfunction exists overall in X-SCID patients and to understand whether the NKT dysfunction is related to the X-SCID clinical symptoms. The present study also characterized the NK cells in this X-SCID patient, which was not discussed in depth in previous studies (17,22), although the findings in this cell type require further investigation due to the low cell number in the patient.

The co-existence of both maternal and autologous T, NKT and NK cells in the patient allowed the present study to explore comprehensively the status and function of both normal and *IL2RG*-mutated cells of these immune cell types in the same microenvironment. When compared with the autologous counterpart, maternal T cells expressed lower level of *GZMK* and *JUN* in Cluster 14 (Fig. 4C) and $CD8^+$ naïve T cells also exhibited differentially expressed genes (Fig. S5A). The two clusters consisted of a small proportion of the total cells, so most of the maternal cells were at a similar cell status to the autologous ones.

The comprehensive comparison with public scRNA-seq data from healthy donors revealed that both maternal engrafted and autologous T, NKT and NK cells in the patient increased the expression of a number of cytokines and type I

interferon responsive genes, suggesting that both maternal and autologous cells fight against recurrent infections in the patient. However, possibly due to the deregulated JAK-STAT pathway (66) in both maternal and autologous cells, the expression of multiple transcription factors mediating the differentiation and activation of T, NKT and NK lymphocytes (*FOS*, *JUN*, *TCF7* and *MYC*) (48-51) was substantially decreased in this X-SCID patient's cells of both origins, consistent with the abnormalities of T, NKT and NK cells previous reported in the X-SCID patients (1,67). Due to the necessity of co-stimulatory molecules for lymphocyte cell proliferation, differentiation, maintenance and activation (68), the deregulation of *CD27*, *CD28* and *CD40LG* in this X-SCID patient's cells from both origins may have contributed to his T cell dysfunction and non-proliferation upon PHA. Notably, the exhaustion-related inhibitory genes *HAVCR2*, *CTLA4* and especially *LAG3* (37-39) were upregulated in the patient's T, NKT and NK cells from both cell origins. *TIGIT* and *PDCD1* were higher in the patient's T cells at both expression and protein levels (Fig. 7A, C and D). This indicated that the T and NK-like cells in this X-SCID patient may have developed an exhausted-like status. In consistence with this result, Okano *et al* (22) reported a higher PD1 protein level in an X-SCID patients with respiratory syncytial virus infection. This is in accordance with reports that both the maternal engrafted cells and autologous cells in SCID are similarly dysfunctional (13,19). Studies with more patients should help to verify if the exhaustion-like state of these immune cells is a common phenomenon in X-SCID patients.

Why were both maternal and autologous cells at a similar cell status? One scenario was that the compromised immunity of the patient was unable to efficiently eliminate foreign viruses and bacteria, resulting in prolonged and recurrent infections and chronic inflammation that may finally exhaust the T and NKT cells. The BMMNC sample in this study was collected when the patient 13 months old, close to the mortality of the patient at 15 months. Maternal engrafted and autologous cells at this time point had both already become exhausted-like due to the recurrent pneumonia and acute hematogenous disseminated tuberculosis, with the maternal cells even more exhausted (Fig. 7C and D). The exhausted-like T cells in the patient limited the expression of *IL2* (Fig. 7B) as in T cell exhaustion defined in other situations (69). Although the maternal T cells in the patient carried the normal *IL2RG* gene, there might be insufficient IL2 ligands produced in the repressed immune state to activate the normal receptor. In this situation, even though the maternal cells exhibit slightly higher level of *IL2RG*, *JAK3* and STAT1-4, the normal *IL2RG* in the maternal cells could not exert its function to completely activate the JAK-STAT signaling pathway.

Except for the mutated *IL2RG* in the autologous cells, the restricted TCR repertoire in maternal T cells (16,70,71) might also contribute to the compromised immunity in the patient. This was supported by the finding in the present study that the gene sets related to TCR diversity were depleted in the patient's T cells (Fig. S6C). Analyses of the TCR repertoire in maternal and autologous T cells using single-cell TCR-seq may help to clarify this possibility. However, 3' scRNA-seq rather than 5' applied in this study impeded the access to the TCR sequences at the 5' end of the TCR genes. Another concern is that due to the low case frequency of X-SCID, the present study collected only this reported case in the past two year. Integrated analyses of larger cohorts of X-SCID patients of different phenotypes prior to and post infections with the 5' scRNA-seq could provide further insights into the common cell status of T and NKT cells and their development in the X-SCID patients.

In conclusion, the present study comprehensively profiled the immune landscape of BMMNCs in an X-SCID patient with maternal engraftment at the single-cell transcriptome level. With the state-of-the-art single-cell sequencing technology, it effectively discriminated the maternal cells from the X-SCID patient autologous ones. The present study revealed the dysfunction of T and NKT cells of both origins contributing to X-SCID symptoms and identified multiple immune signatures involved in T and NKT lymphocyte dysfunction and exhaustion. These results might provide new insights into the mechanisms underlying X-SCID pathogenesis and could contribute to the early diagnosis of SCID patients.

Acknowledgements

Not applicable.

Funding

The present study was supported by grants from the National Natural Science Foundation of China (grant no. 31900415), Research Foundation of Guangzhou Women and Children's Medical Center for Clinical Doctor (grant no. 1600071) and Guangzhou Basic Research Plan of Basic and Applied Basic Research Foundation (grant no. 202201011221).

Availability of data and materials

The single-cell RNA sequencing data of the X-SCID patient in this study has been deposited in the GSA database (Genome Sequence Archive in BIG Data Center, Beijing Institute of Genomics, Chinese Academy of Sciences) under the accession number HRA000811 (accessible at http://bigd.big.ac.cn/gsa-human). The bulk WGS and captured exome sequencing data were also deposited in the GSA database, under the accession number HRA001493. All other data generated or analyzed during this study are included in this published article. Supplementary Information is available from the corresponding authors on reasonable request. The scripts generated during this study are available at the GitHub repository (https://github.com/dongwei1220/X-SCID_scRNA-seq).

Authors' contributions

GL, XW and ZT designed and supervised the study. WD performed the data analysis and interpretation. HF and XW collected the clinical samples, XW and XZ prepared the scRNA-seq libraries. WL, SZ, QQ and XW performed the FACS experiment. WD, XW and WL wrote the manuscript and other co-authors critically reviewed and modified the manuscript. LG and XW confirm the authenticity of all the raw data. All authors read and approved the final manuscript.

Ethics approval and consent to participate

Informed consents for the performed studies were obtained from the patient's parents, in accordance with the principles of the ethics committee of the Guangzhou Women and Children's Medical Center (approval number: 105A01).

Patient consent for publication

Not applicable.

Competing interests

The authors declare that they have no competing interests.

References

1. Fischer A: Severe combined immunodeficiencies (SCID). Clin Exp Immunol 122: 143-149, 2000.
2. Notarangelo LD: Primary immunodeficiencies. J Allergy Clin Immunol 125 (2 Suppl 2): S182-S194, 2010.
3. Cirillo E, Giardino G, Gallo V, D'Assante R, Grasso F, Romano R, Lillo CD, Galasso G and Pignata C: Severe combined immunodeficiency-an update. Ann N Y Acad Sci 1356: 90-106, 2015.
4. Fazlollahi MR, Pourpak Z, Hamidieh AA, Movahedi M, Houshmand M, Badalzadeh M, Nourizadeh M, Mahloujirad M, Arshi S, Nabavi M, *et al*: Clinical, laboratory, and molecular findings for 63 patients with severe combined immunodeficiency: A decade s experience. J Investig Allergol Clin Immunol 27: 299-304, 2017.
5. Tangye SG, Al-Herz W, Bousfiha A, Chatila T, Cunningham-Rundles C, Etzioni A, Franco JL, Holland SM, Klein C, Morio T, *et al*: Human inborn errors of immunity: 2019 update on the classification from the international union of immunological societies expert committee. J Clin Immunol 40: 24-64, 2020.
6. Noguchi M, Yi H, Rosenblatt HM, Filipovich AH, Adelstein S, Modi WS, McBride OW and Leonard WJ: Interleukin-2 receptor gamma chain mutation results in X-linked severe combined immunodeficiency in humans. Cell 73: 147-157, 1993.
7. Russell SM, Johnston JA, Noguchi M, Kawamura M, Bacon CM, Friedmann M, Berg M, McVicar DW, Witthuhn BA and Silvennoinen O: Interaction of IL-2R beta and gamma c chains with Jak1 and Jak3: Implications for XSCID and XCID. Science 266: 1042-1045, 1994.
8. Kovanen PE and Leonard WJ. Cytokines and immunodeficiency diseases: Critical roles of the gamma (c)-dependent cytokines interleukins 2, 4, 7, 9, 15, and 21, and their signaling pathways. Immunol Rev 202: 67-83, 2004.
9. Niemela JE, Puck JM, Fischer RE, Fleisher TA and Hsu AP: Efficient detection of thirty-seven new IL2RG mutations in human X-linked severe combined immunodeficiency. Clin Immunol 95: 33-38, 2000.
10. Chong HJ, Maurer S and Heimall J: What to do with an abnormal newborn screen for severe combined immune deficiency. Immunol Allergy Clin North Am 39: 535-546, 2019.
11. Myers LA, Patel DD, Puck JM and Buckley RH: Hematopoietic stem cell transplantation for severe combined immunodeficiency in the neonatal period leads to superior thymic output and improved survival. Blood 99: 872-878, 2002.
12. Muller SM, Ege M, Pottharst A, Schulz AS, Schwarz K and Friedrich W: Transplacentally acquired maternal T lymphocytes in severe combined immunodeficiency: A study of 121 patients. Blood 98: 1847-1851, 2001.
13. Kellermayer R, Hsu AP, Stankovics J, Balogh P, Hadzsiev K, Vojcek A, Maródi L, Kajtár P, Kosztolányi G and Puck JM: A novel IL2RG mutation associated with maternal T lymphocyte engraftment in a patient with severe combined immunodeficiency. J Hum Genet 51: 495-497, 2006.
14. Tezcan I, Ersoy F, Sanal O, Turul T, Uckan D, Balci S, Hicsonmez G, Prieur M, Caillat-Zucmann S, Le Deist F and De Saint Basile G: Long-term survival in severe combined immune deficiency: The role of persistent maternal engraftment. J Pediatr 146: 137-140, 2005.
15. van der Burg M and Gennery AR: Educational paper. The expanding clinical and immunological spectrum of severe combined immunodeficiency. Eur J Pediatr 170: 561-571, 2011.
16. Lev A, Simon AJ, Trakhtenbrot L, Goldstein I, Nagar M, Stepensky P, Rechavi G, Amariglio N and Somech R: Characterizing T cells in SCID patients presenting with reactive or residual T lymphocytes. Clin Dev Immunol 2012: 261470, 2012.
17. Touzot F, Dal-Cortivo L, Verkarre V, Lim A, Crucis-Armengaud A, Moshous D, Héritier S, Frange P, Kaltenbach S, Blanche S, *et al*: Massive expansion of maternal T cells in response to EBV infection in a patient with SCID-Xl. Blood 120: 1957-1959, 2012.
18. Denianke KS, Frieden IJ, Cowan MJ, Williams ML and McCalmont TH: Cutaneous manifestations of maternal engraftment in patients with severe combined immunodeficiency: A clinicopathologic study. Bone Marrow Transplant 28: 227-233, 2001.
19. Thompson LF, O'Connor RD and Bastian JF: Phenotype and function of engrafted maternal T cells in patients with severe combined immunodeficiency. J Immunol 133: 2513-2517, 1984.
20. Kobrynski LJ and Abramowsky C: Monoclonal IgA gammopathy due to maternal B cells in an infant with severe combined immunodeficiency (SCID) prior to hematopoietic stem cell transplantation. J Pediatr Hematol Oncol 28: 53-56, 2006.
21. Morinishi Y, Imai K, Nakagawa N, Sato H, Horiuchi K, Ohtsuka Y, Kaneda Y, Taga T, Hisakawa H, Miyaji R, *et al*: Identification of severe combined immunodeficiency by T-cell receptor excision circles quantification using neonatal guthrie cards. J Pediatr 155: 829-833, 2009.
22. Okano T, Nishikawa T, Watanabe E, Watanabe T, Takashima T, Yeh TW, Yamashita M, Tanaka-Kubota M, Miyamoto S, Mitsuiki N, *et al*: Maternal T and B cell engraftment in two cases of X-linked severe combined immunodeficiency with IgG1 gammopathy. Clin Immunol 183: 112-120, 2017.
23. Bolger AM, Lohse M and Usadel B: Trimmomatic: A flexible trimmer for Illumina sequence data. Bioinformatics 30: 2114-2120, 2014.
24. Li H and Durbin R: Fast and accurate short read alignment with burrows-wheeler transform. Bioinformatics 25: 1754-1760, 2009.
25. Li H, Handsaker B, Wysoker A, Fennell T, Ruan J, Homer N, Marth G, Abecasis G and Durbin R; 1000 Genome Project Data Processing Subgroup: The sequence alignment/map format and SAMtools. Bioinformatics 25: 2078-2079, 2009.
26. Robinson JT, Thorvaldsdottir H, Wenger AM, Zehir A and Mesirov JP: Variant review with the integrative genomics viewer. Cancer Res 77: e31-e34, 2017.
27. Robinson JT, Thorvaldsdottir H, Winckler W, Guttman M, Lander ES, Getz G and Mesirov JP: Integrative genomics viewer. Nat Biotechnol 29: 24-26, 2011.
28. Thorvaldsdottir H, Robinson JT and Mesirov JP: Integrative genomics viewer (IGV): High-performance genomics data visualization and exploration. Brief Bioinform 14: 178-192, 2013.
29. R Core Team (2020). R: A language and environment for statistical computing. R Foundation for Statistical Computing, Vienna, Austria. URL https://www.R-project.org/.
30. Stuart T, Butler A, Hoffman P, Hafemeister C, Papalexi E, Mauck WM III, Hao Y, Stoeckius M, Smibert P and Satija R: Comprehensive integration of single-cell data. Cell 177: 1888-1902 e21, 2019.
31. Aran D, Looney AP, Liu L, Wu E, Fong V, Hsu A, Chak S, Naikawadi RP, Wolters PJ, Abate AR, *et al*: Reference-based analysis of lung single-cell sequencing reveals a transitional profibrotic macrophage. Nat Immunol 20: 163-172, 2019.
32. Novershtern N, Subramanian A, Lawton LN, Mak RH, Haining WN, McConkey ME, Habib N, Yosef N, Chang CY, Shay T, *et al*: Densely interconnected transcriptional circuits control cell states in human hematopoiesis. Cell 144: 296-309, 2011.
33. Yu G, Wang LG, Han Y and He QY: clusterProfiler: An R package for comparing biological themes among gene clusters. OMICS 16: 284-287, 2012.
34. Ashburner M, Ball CA, Blake JA, Botstein D, Butler H, Cherry JM, Davis AP, Dolinski K, Dwight SS, Eppig JT, *et al*: Gene ontology: Tool for the unification of biology. The gene ontology consortium. Nat Genet 25: 25-29, 2000.
35. Gene Ontology Consortium: The gene ontology resource: Enriching a GOld mine. Nucleic Acids Res 49: D325-D334, 2021.
36. Li J, Miao B, Wang S, Dong W, Xu H, Si C, Wang W, Duan S, Lou J, Bao Z, *et al*: Hiplot: A comprehensive and easy-to-use web service for boosting publication-ready biomedical data visualization. Brief Bioinform 23: bbac261, 2022.

37. Catakovic K, Klieser E, Neureiter D and Geisberger R: T cell exhaustion: From pathophysiological basics to tumor immunotherapy. Cell Commun Signal 15: 1, 2017.
38. Huang YH, Zhu C, Kondo Y, Anderson AC, Gandhi A, Russell A, Dougan SK, Petersen BS, Melum E, Pertel T, *et al*: CEACAM1 regulates TIM-3-mediated tolerance and exhaustion. Nature 517: 386-390, 2015.
39. Ruffo E, Wu RC, Bruno TC, Workman CJ and Vignali DAA: Lymphocyte-activation gene 3 (LAG3): The next immune checkpoint receptor. Semin Immunol 42: 101305, 2019.
40. Khan O, Giles JR, McDonald S, Manne S, Ngiow SF, Patel KP, Werner MT, Huang AC, Alexander KA, Wu JE, *et al*: TOX transcriptionally and epigenetically programs CD8 (+) T cell exhaustion. Nature 571: 211-218, 2019.
41. Kim K, Park S, Park SY, Kim G, Park SM, Cho JW, Kim DH, Park YM, Koh YW, Kim HR, *et al*: Single-cell transcriptome analysis reveals TOX as a promoting factor for T cell exhaustion and a predictor for anti-PD-1 responses in human cancer. Genome Med 12: 22, 2020.
42. Seo H, Chen J, Gonzalez-Avalos E, Samaniego-Castruita D, Das A, Wang YH, López-Moyado IF, Georges RO, Zhang W, Onodera A, *et al*: TOX and TOX2 transcription factors cooperate with NR4A transcription factors to impose CD8 (+) T cell exhaustion. Proc Natl Acad Sci USA 116: 12410-12415, 2019.
43. Aibar S, Gonzalez-Blas CB, Moerman T, Huynh-Thu VA, Imrichova H, Hulselmans G, Rambow F, Marine JC, Geurts P, Aerts J, *et al*: SCENIC: Single-cell regulatory network inference and clustering. Nat Methods 14: 1083-1086, 2017.
44. Liberzon A, Birger C, Thorvaldsdottir H, Ghandi M, Mesirov JP and Tamayo P: The molecular signatures database (MSigDB) hallmark gene set collection. Cell Syst 1: 417-425, 2015.
45. Pepper AE, Buckley RH, Small TN and Puck JM: Two mutational hotspots in the interleukin-2 receptor gamma chain gene causing human X-linked severe combined immunodeficiency. Am J Hum Genet 57: 564-571, 1995.
46. Brown CJ, Ballabio A, Rupert JL, Lafreniere RG, Grompe M, Tonlorenzi R and Willard HF: A gene from the region of the human X inactivation centre is expressed exclusively from the inactive X chromosome. Nature 349: 38-44, 1991.
47. Brown CJ, Hendrich BD, Rupert JL, Lafreniere RG, Xing Y, Lawrence J and Willard HF: The human XIST gene: Analysis of a 17 kb inactive X-specific RNA that contains conserved repeats and is highly localized within the nucleus. Cell 71: 527-542, 1992.
48. Hatakeyama M, Kawahara A, Mori H, Shibuya H and Taniguchi T: c-fos gene induction by interleukin 2: Identification of the critical cytoplasmic regions within the interleukin 2 receptor beta chain. Proc Natl Acad Sci USA 89: 2022-2026, 1992.
49. Kawahara A, Minami Y, Miyazaki T, Ihle JN and Taniguchi T: Critical role of the interleukin 2 (IL-2) receptor gamma-chain-associated Jak3 in the IL-2-induced c-fos and c-myc, but not bcl-2, gene induction. Proc Natl Acad Sci USA 92: 8724-8728, 1995.
50. Wu JQ, Seay M, Schulz VP, Hariharan M, Tuck D, Lian J, Du J, Shi M, Ye Z, Gerstein M, *et al*: Tcf7 is an important regulator of the switch of self-renewal and differentiation in a multipotential hematopoietic cell line. PLoS Genet 8: e1002565, 2012.
51. Xing S, Li F, Zeng Z, Zhao Y, Yu S, Shan Q, Li Y, Phillips FC, Maina PK, Qi HH, *et al*: Tcf1 and Lef1 transcription factors establish CD8 (+) T cell identity through intrinsic HDAC activity. Nat Immunol 17: 695-703, 2016.
52. Decaluwe H, Taillardet M, Corcuff E, Munitic I, Law HK, Rocha B, Rivière Y and Di Santo JP: Gamma (c) deficiency precludes CD8+ T cell memory despite formation of potent T cell effectors. Proc Natl Acad Sci USA 107: 9311-9216, 2010.
53. He Y, Xiao R, Ji X, Li L, Chen L, Xiong J, Xiao W, Wang Y, Zhang L, Zhou R, *et al*: EBV promotes human CD8 NKT cell development. PLoS Pathog 6: e1000915, 2010.
54. Zenz R, Eferl R, Scheinecker C, Redlich K, Smolen J, Schonthaler HB, Kenner L, Tschachler E and Wagner EF: Activator protein 1 (Fos/Jun) functions in inflammatory bone and skin disease. Arthritis Res Ther 10: 201, 2008.
55. Wagner EF and Eferl R: Fos/AP-1 proteins in bone and the immune system. Immunol Rev 208: 126-140, 2005.
56. Jin HT, Anderson AC, Tan WG, West EE, Ha SJ, Araki K, Freeman GJ, Kuchroo VK and Ahmed R: Cooperation of Tim-3 and PD-1 in CD8 T-cell exhaustion during chronic viral infection. Proc Natl Acad Sci USA 107: 14733-1478, 2010.
57. Allenspach E, Rawlings DJ, Petrovic A, Chen K, Adam MP, Everman DB, Mirzaa GM, Pagon RA, Wallace SE, Bean LJH, *et al*: X-linked severe combined immunodeficiency. In: editors. GeneReviews ((R)). Seattle (WA)1993.
58. Recher M, Berglund LJ, Avery DT, Cowan MJ, Gennery AR, Smart J, Peake J, Wong M, Pai SY, Baxi S, *et al*: IL-21 is the primary common gamma chain-binding cytokine required for human B-cell differentiation in vivo. Blood 118: 6824-6835, 2011.
59. Lee PP, Chan KW, Chen TX, Jiang LP, Wang XC, Zeng HS, Chen XY, Liew WK, Chen J, Chu KM, *et al*: Molecular diagnosis of severe combined immunodeficiency-identification of IL2RG, JAK3, IL7R, DCLRE1C, RAG1, and RAG2 mutations in a cohort of Chinese and Southeast Asian children. J Clin Immunol 31: 281-296, 2011.
60. Shibata F, Toma T, Wada T, Inoue M, Tone Y, Ohta K, Kasahara Y, Sano F, Kimura M, Ikeno M, *et al*: Skin infiltration of CD56 (bright) CD16 (-) natural killer cells in a case of X-SCID with Omenn syndrome-like manifestations. Eur J Haematol 79: 81-85, 2007.
61. Randles LG, Lappalainen I, Fowler SB, Moore B, Hamill SJ and Clarke J: Using model proteins to quantify the effects of pathogenic mutations in Ig-like proteins. J Biol Chem 281: 24216-24226, 2006.
62. Notarangelo LD, Giliani S, Mazza C, Mella P, Savoldi G, Rodriguez-Perez C, Mazzolari E, Fiorini M, Duse M, Plebani A, *et al*: Of genes and phenotypes: The immunological and molecular spectrum of combined immune deficiency. Defects of the gamma (c)-JAK3 signaling pathway as a model. Immunol Rev 178: 39-48, 2000.
63. Puck JM, Pepper AE, Henthorn PS, Candotti F, Isakov J, Whitwam T, Conley ME, Fischer RE, Rosenblatt HM, Small TN and Buckley RH: Mutation analysis of IL2RG in human X-linked severe combined immunodeficiency. Blood 89: 1968-1977, 1997.
64. Heaton H, Talman AM, Knights A, Imaz M, Gaffney DJ, Durbin R, Hemberg M and Lawniczak MKN: Souporcell: Robust clustering of single-cell RNA-seq data by genotype without reference genotypes. Nat Methods 17: 615-620, 2020.
65. Palmer K, Green TD, Roberts JL, Sajaroff E, Cooney M, Parrott R, Chen DF, Reinsmoen NL and Buckley RH: Unusual clinical and immunologic manifestations of transplacentally acquired maternal T cells in severe combined immunodeficiency. J Allergy Clin Immunol 120: 423-438, 2007.
66. Leonard WJ, Lin JX and O'Shea JJ: The gammac family of cytokines: Basic biology to therapeutic ramifications. Immunity 50: 832-850, 2019.
67. Wiekmeijer AS, Pike-Overzet K, IJspeert H, Brugman MH, Wolvers-Tettero IL, Lankester AC, Bredius RGM, van Dongen JJM, Fibbe WE, Langerak AW, *et al*: Identification of checkpoints in human T-cell development using severe combined immunodeficiency stem cells. J Allergy Clin Immunol 137: 517-526 e3, 2016.
68. Chen L and Flies DB: Molecular mechanisms of T cell co-stimulation and co-inhibition. Nat Rev Immunol 13: 227-242, 2013.
69. Wherry EJ: T cell exhaustion. Nat Immunol 12: 492-499, 2011.
70. Plebani A, Stringa M, Prigione I, Facchetti P, Ghiotto F, Airoldi I, Giacchino R, Cristina E, Porta F, Grossi CE and Pistoia V: Engrafted maternal T cells in human severe combined immunodeficiency: Evidence for a TH2 phenotype and a potential role of apoptosis on the restriction of T-cell receptor variable beta repertoire. J Allergy Clin Immunol 101: 131-134, 1998.
71. Knobloch C, Goldmann SF and Friedrich W: Limited T cell receptor diversity of transplacentally acquired maternal T cells in severe combined immunodeficiency. J Immunol 146: 4157-4164, 1991.